Published in final edited form as:
J Neuropathol Exp Neurol. 2012 August ; 71(8): 729–740. doi:10.1097/NEN.0b013e3182625c02.

Cell of Origin Determines Tumor Phenotype in an Oncogenic Ras/p53 Knockout Transgenic Model of High-Grade Glioma

Sabah O. Ghazi, PhD[1], **Michelle Stark, BS**[1], **Zhiguo Zhao, MS**[2], **Bret C. Mobley, MS, MD**[1], **Alex Munden, BS**[1], **Laura Hover, BS**[1], and **Ty W. Abel, MD, PhD**[1]

[1]Department of Pathology, Vanderbilt University Medical Center Nashville, Tennessee

[2]Department of Biostatistics, Vanderbilt University Medical Center Nashville, Tennessee

Abstract

Human high-grade gliomas (HGGs) are known for their histologic diversity. To address the role of cell of origin in glioma phenotype, transgenic mice were generated in which oncogenic Ras and p53 deletion were targeted to neural stem/progenitor cells (NSPCs) as well as mature astrocytes. *hGFAP-Cre/Kras*^{G12D}*/p53*$^{fl/fl}$ mice develop multifocal HGG that vary histopathologically and with respect to the expression of markers associated with NSPCs. One HGG pattern strongly expressed markers of NSPCs and arose near the subventricular zone. Additional, non-overlapping patterns that recapitulate human HGG variants were present simultaneously in the same brain. These neoplastic foci were more often cortical- or leptomeningeal-based and the neoplastic cells lacked expression of NSPC markers. To determine whether cell of origin determines tumor phenotype, astrocytes and NSPCs were harvested from neonatal mutant pups. Upon orthotopic transplantation, early-passage astrocytes and NSPCs formed tumors that differed in engraftment rates, latency to clinical signs, histopathology and protein expression. Astrocyte-derived tumors were more aggressive had giant cell histology and glial fibrillary acidic protein expression. NSPC-derived tumors retained NSPC markers and showed evidence of differentiation along astrocytic, oligodendroglial, and neuronal lineages. These results indicate that identical tumorigenic stimuli produce markedly different glioma phenotypes depending on the differentiation status of the transformed cell.

Keywords

GFAP-Cre; Glioma; High-grade glioma; *Kras*; Neural stem/progenitor cells; *p53*; Transgenic mice

INTRODUCTION

High-grade gliomas (HGGs) constitute the most common type of primary CNS neoplasm. Well known for their histologic heterogeneity, these highly infiltrative neoplasms are associated with a dismal prognosis despite surgery, radiotherapy, and chemotherapy. Many histologic subtypes of HGGs have been described, including giant cell (1, 2), gemistocytic (3), gliosarcoma (4, 5), and small cell variants (6). The mechanisms underlying this striking histologic heterogeneity in HGGs have not been adequately explained.

Send correspondence and reprint requests to: Ty W. Abel, MD, PhD, Department of Pathology, Vanderbilt University Medical Center, 1161 21st Ave South, MCN C2318, Nashville, TN, 37232. Phone: 615-771-9684; Fax: 615-343-7089; ty.w.abel@vanderbilt.edu.

Cushing and Bailey postulated 85 years ago that transformation of neural precursor cells leads to tumors with divergent differentiation (7). The more recent observation that neural stem/precursor cells (NSPCs) persist in the adult, mammalian brain lends credence to this hypothesis (8, 9), as does the presence of neoplastic cells with stem cell-like properties in human HGG (10–15). Furthermore, recent studies demonstrate that at least 3 subtypes of HGG exist; gliomas in patients with relatively prolonged survival are distinguished by patterns of gene expression associated with the process of neural differentiation (16). Distinguishing those gliomas that arise from multipotent precursor cells vs. those that may arise from fully differentiated astrocytes may influence current glioma classification, as well as prognosis and treatment.

By targeting particular cell populations in the developing and adult brain, transgenic mouse models provide a means to address the mechanisms underlying the histologic and molecular heterogeneity of gliomas. Although it has proven difficult to target NSPCs specifically and exclusively, several groups have provided evidence that oncogenic transformation of these cells leads to glioma (17–21). For example, our group recently reported that targeting oncogenic Ras ($Kras^{G12D}$) to NSPC is sufficient to produce marked hyperplasia of the subventricular zone (SVZ), a major NSPC population in the brain (18). In addition, the targeted mice develop multifocal, infiltrating, intermediate-grade gliomas that often arise near the expanded SVZ. Furthermore, the tumor cells expressed markers associated with NSPC and glioma stem cells, including Olig2, Bmi-1, and platelet-derived growth factor α.

Although data suggest that NSPCs may be important in gliomagenesis, there are few detailed comparisons of experimental gliomas derived from NSPCs and more mature cell types in the literature. If the cell of origin determines, at least in part, histologic diversity in gliomas, tumors that arise from transformed NSPC should be demonstrably different from those derived from more mature cells that harbor identical genetic manipulations. Here, using *hGFAP-Cre* transgenic mice, in which Cre expression is targeted to NSPCs as well as mature astrocytes, we describe multiple, simultaneous, HGG phenotypes with activation of $Kras^{G12D}$ and concomitant, homozygous deletion of p53. One HGG subtype was distinguished from other patterns by proximity to the ventricles/SVZ and by expression of neural/glioma stemness markers. To test the hypothesis that the differentiation status of the cell of origin influences tumor phenotype, we isolated NSPC and mature astrocytes from $hGFAP\text{-}Cre/Kras^{G12D}/p53^{fl/fl}$ mutant pups. In an orthotopic transplant model, we show distinct differences in survival, histology, and protein expression between tumors that arose from transformed, orthotopically injected NSPCs vs. those that arose from transformed astrocytes.

MATERIALS AND METHODS

Transgenic Mice

$Kras^{G12D}$ mice were a gift from Dr. Tyler Jacks, Massachusetts Institute of Technology, Cambridge, MA. In these mice, oncogenic *Kras* ($Kras^{G12D}$) is targeted to the endogenous K-ras locus (22). The allele is silenced by a stop codon flanked by loxP sites. Cre recombinase–mediated excision of the stop cassette results in expression of the transgene from the endogenous *Kras* promoter. *hGFAP-Cre* mice [FVB-Tg (GFAP-cre) 25Mes/J] and conditional $p53^{fl/fl}$ (B6.129P2-Trp53tm1Brn/J) mice were obtained from The Jackson Laboratory, Bar Harbor, ME. Polymerase chain reaction (PCR) was used to identify the presence of the *GFAP-Cre* and $Kras^{G12D}$ alleles in tail DNA using oligonucleotide primers as previously described (22, 23). The primers for detection of the floxed p53 allele were as follows: 5'-GGTTAAACCCAGCTTGACCA-3 and 5'-GGAGGCAGAGACAGTTGGAG-3'. $p53^{fl/fl}$ mice were mated with $Kras^{G12D}$ mice (129/SvJac/C57BL/6) to generate $p53^{fl/fl}/K\text{-}ras^{G12D}$ mice. *GFAP-Cre* mice were then bred to

p53$^{fl/fl}$/*Kras*^{G12D} mice to generate *GFAP-Cre/Kras*^{G12D}/*p53*$^{flox/flox}$ mice on a mixed background. Mice were housed in the animal care facility at Vanderbilt University following the Association for Assessment and Accreditation of Laboratory Animal Care guidelines. All animal procedures were approved by the Vanderbilt Institutional Animal Care and Use Committee.

Histology, Immunohistochemistry, and Immunofluorescence

Mice were killed and their brains were fixed in 10% buffered formalin acetate overnight, followed by fixation in 70% ethanol. A mid-sagittal cut separated the hemispheres. Additional parasagittal sections were generated from one hemisphere, and the opposite hemisphere was sectioned in the coronal plane. Tissue sections were embedded in paraffin and sectioned at 5μm. The sections were stained with hematoxylin and eosin. Immunohistochemical staining was performed using the following protocol: Sections measuring 5 μm from paraffin-embedded specimens were mounted on glass slides, dried overnight at 37°C. Sections were deparaffinized in xylene and washed in a graded series of ethanol. Endogenous peroxidase activity was quenched in 3% H2O2 for 10 minutes. Sections were then boiled in 100 mM citrate buffer (pH 6.0) for 10 minutes. The slides were blocked for non-specific binding using normal goat serum (Vector Laboratories, Burlingame, CA). The sections were also blocked for biotin and avidin using Biotin/Avidin system (Vector Laboratories). The slides were incubated with primary antibodies raised against Nestin (Millipore, Billerica, MA, 1:1000), Olig2 (Millipore, 1:500), Sox2 (Millipore, 1:8000), Bmi-1 (Millipore, 1:200), Ki67 (Vector Laboratories,1:100), glial fibrillary acidic protein ([GFAP], Santa Cruz Biotechnology, Santa Cruz, CA, 1:100), and phospho-histone-H3 (pH-3, Millipore, 1:3000). Sections were incubated with primary antibodies overnight at 4°C. After washing the slides with TBST, the appropriate secondary antibodies were applied for 30 minutes. For anti-mouse primaries the M.O.MTM Kit was used (Vector Laboratories). The sections were washed and incubated for 30 minutes with VECTASTAIN Elite ABC reagent; NovaRED substrate kit (Vector Laboratories) was used for color visualization. The sections were counterstained with hematoxylin and coverslipped.

For immunofluorescent studies, astrocytes were cultured on 22×22 mm coverslips, washed with PBS and then fixed with 4% sucrose and 4% paraformaldehyde for 30 minutes at room temperature. Cells were then washed twice with PBS for 5 minutes each and permeabilized with 0.2% TritonX-100 for 30 minutes. Cultured neurospheres were first embedded in HistoGelTM (Richard-Allen Scientific, Kalamazoo, MI), then in paraffin and sectioned at 5 μm. The sections were deparaffinized and processed as above. For immunostaining, both astrocytes and neurospheres were blocked with normal goat serum (Vector Laboratories) and incubated in the primary antibodies raised against nestin (1:100), Olig2 (1:500), Sox2 (1000), and GFAP (Dako, Carpinteria, CA, 1:750). Cells were incubated with the primary antibodies overnight at 4°C. The slides were washed with phosphate buffered saline with Tween and incubated in the appropriate secondary antibodies (1:750), i.e. Alexa Flour 488 for anti-mouse and Alexa Flour 594 for anti-Rabbit (Invitrogen, Grand Island, NY). Cells were then mounted using ProLong Gold anti-fade reagent with 4',6-diamidino-2-phenylindole ([DAPI], Invitrogen).

Mitoses per high-power field (HPF) were counted by an observer blinded to the source (astrocyte or NSPC) of the tumor. Tumors from 3 animals in each group were stained for the mitosis marker p-H3. Mitoses were counted in 30 HPF per tumor. The mean number of mitoses per HPF was calculated for each tumor and a grand mean was calculated for the group.

Western Blotting Analysis

Astrocytes and neurospheres or brain tumor tissue were lysed in RIPA buffer (50 mM Tris HCl [pH 8.0];150 mM NaCl; 1% Triton X-100; 0.5% sodium deoxycholate; 0.1% SDS; 1 mM EDTA; 0.5 mM PMSF; 1 mM NaF; 0.2% phosphatase inhibitor cocktail (Sigma, St. Louis, MO, 50 ug/mL leupeptin). Approximately 25 ug of protein from each sample was loaded for SDS-PAGE and transferred to PVDF membrane. Membranes were blocked in 7% TBST-milk for 1 h at 25°C. The PVDF was immunoblotted with specific primary antibodies with an overnight incubation at 4°C in the primary antibodies. Secondary antibodies were added for 1 hour at 25°C. Proteins were visualized using a chemiluminescent detection system (PerkinElmer, Waltham, MA). Primary antibodies used included nestin (1:2500), Olig2 (1:1000), Sox2 (1:1000), Bmi-1 (1:5000), and GFAP (Stemcell Technologies, Vancouver, Canada, 1:5000). Horseradish peroxidase-conjugated secondary antibodies were used: anti-rabbit IgG (Promega, Madison, WI 1:5000), and anti-mouse IgG (Promega, 1:5000). β-actin (Sigma Aldrich, 1: 5000) levels were determined for each condition to verify that equal amounts of protein were loaded.

Astrocyte and NSPC Cultures

Astrocytes and neurospheres were harvested from neonatal (less than 7 days old) *GFAP-Cre/Kras^{G12D}/p53$^{fl/fl}$* pups and appropriate control pups. The pups were killed, the brains were removed, and the tissue was placed in Dulbecco's phosphate buffered saline (DPBS) at 4°C with 4.5 g/L glucose (DPBS/glu). For neurosphere cultures, the forebrain periventricular region including the SVZ was dissected. Astrocytes were harvested from cortical brain tissue. In both cases, tissue was transferred to fresh DPBS/glu, washed once, and then mechanically dissociated. Neurospheres were grown in NeuroCult Basal Medium (Stemcell Technologies), supplemented with 0.1 g/L penicillin/streptomycin, 2 μg/ml heparin, 10 ng/ml basic fibroblast growth factor and 20 ng/ml epidermal growth factor (EGF) and in the absence of serum. Astrocytes were grown in DMEM/F12 containing 2 mM L-glutamine and 0.1 g/L penicillin/streptomycin, 10% fetal bovine serum and 20 ug/mL EGF. DNA was extracted from cultured astrocytes and neurospheres, and PCR was performed to detect the recombined K-rasG12D allele using the following primers: 5'-GGGTAGGTGTTGGGATAGCTG-3' and 5'-TCCGAATTCAGTGACTACAGATGTACAGAG-3'.

Quantitative Real-Time PCR

Astrocytes and NSPCs were seeded at 500,000 cells/well in 6-well plates. For comparison of gene expression between mutant NSPCs and astrocytes and between NSPCs in the presence and absence of serum, NSPCs were harvested and grown in serum-free stem cell medium (as above). The cells were then placed in astrocyte medium (as above) for 5 days. Cells were lysed using the RNeasy mini kit (Qiagen, Valencia, CA). cDNA was synthesized using the SuperScript Vilo cDNA synthesis kit (Invitrogen). All reactions were performed in triplicate, and each sample was normalized with the threshold cycle of glyceraldehyde-3-phosphate dehydrogenase to obtain the Δ cycle threshold (Ct) value. CYBR Green fluorochrome was used to perform the real-time PCR reaction. Standard curve was obtained to calculate the Ct values to obtain gene expression values and graphs. The PCR primers were as follows:

GFAP: Forward: 5'-TGGAGGGCGAAGAAAACCGCA-3'

Reverse: 5'-GGTGCTTTTGCCCCCTCGGAT-3'

Sox2: Forward: 5'-TGCTGCCTCTTTAAGACTAGGGCTG-3'

Reverse: 5'-GGCCGCCGCGATTGTTGTGA-3'

Olig2: Forward: 5’- GCGGAACCCCGAAAGGTGTG -3’

Reverse: 5’- TTTGAGGTGCTCGCTGCGGA -3’

Nestin: Forward: 5’- AGTGCTCCACGTCCGCTTGC -3’

Reverse: 5’- AGGTAGGCCTCCAGGCGTCG -3’

Tuj1: Forward: 5’- AGCCGCGTGAAGTCAGCATGAG-3’

Reverse: 5’- CCGCTGGGGTCTATGCCGTG-3’

Delta-like ligand 3: Forward: 5’- GGCGCCGCACTCTTGGTCAT -3’

Reverse: 5’- GCGTGTGGACCGAAGGCTCC -3’

Bcan: Forward: 5’- CGGCGTGAACCTGCAGAGCA -3’

Reverse: 5’- GGTTGCGGTCGCAGCGGTAT -3’

VEGF: Forward: 5’- CAGAGGCTTGGGGCAGCCG -3’

Reverse: 5’- TGCCTTGTCGCTGCGTCTCG -3’

CD44: Forward: 5’- AGCACCTTGGCCACCACTCCT-3’

Reverse: 5’- GGGGTTCTTCCCCTGCCATCC -3’

CHI3L1/YKL-40

Forward: 5’- ACGCACTGCTTTCGTCCGGT -3’

Reverse: 5’- GCCAGGCGAGATCCAGCCCA -3’

Myelin Basic Protein (MBP): Forward: 5’- AGCGGGGCTCTGGCAAGGTA -3’

Reverse: 5’- GACGGCTGCGGGCATGAGAG -3’

S100B: Forward: 5’- AGCTCCCGGGATGTCCGAGC -3’

Reverse: 5’- GTCACCCTCTCGCCCGGAGT -3’

Orthotopic Transplants

Adult mice were anesthetized with a ketamine (100 mg/kg) and xylazine (10 mg/kg) mixture. Using a stereotactic frame (Kopf Instruments, Tujunga, CA), 100,000 dissociated neurospheres or differentiated astrocytes (resuspended in 2.5 μl of media) were implanted into the left corpus striatum at depth of 2.5 mm from the dural surface. The animals were monitored for neurological signs or weight loss for at least 180 days and killed if there was significant neurological dysfunction or 20% weight loss.

Statistical Analyses

The moderated t-statistic implemented in the Bioconductor LIMMA package was used to detect differentially expressed genes between NSPCs in the presence and absence of serum and between NSPCs and astrocytes in serum. This statistic has the same interpretation as the standard t-statistic; however, the standard errors were calculated to shrink toward a common value by the empirical Bayes model to borrow information across all genes (24). To control for false discovery rates, p values for moderated t tests were adjusted using the method of Benjamini and Hochberg (25). All quantitative RT-PCR data analyses were performed using R 2.13.1 (R Development Core Team, Vienna, Austria). A significance level of 0.05 was used for statistical inference unless otherwise noted. Survival analysis was performed using GraphPad Prism software. Student t-test was used to assess differences in tumor mitotic

activity between groups of mice. Differences in engraftment rates were evaluated by Fisher exact test.

RESULTS

hGFAP-Cre-Mediated Recombination of *Kras^{G12D}* and Homozygous Deletion of p53 Results in Multiple, Simultaneous, HGG Phenotypes

Kras^{G12D} mice were mated with *p53$^{fl/fl}$* mice and *hGFAP-Cre* mice to produce trigenic, *hGFAP-Cre/ Kras^{G12D}/p53$^{fl/fl}$* mice. These pups were macroscopically normal at birth and in the early postnatal period. By approximately 2 weeks of age they were distinguished from littermate controls by a peculiar skin abnormality. The abnormality is likely due to *GFAP-Cre* expression in skin, as evidenced by β-galactosidase activity in the skin of *GFAP-Cre/ Rosa26r* mice (data not shown). The skin is characterized grossly by transverse bands of alopecia. Some mice developed skin tumors in the first several weeks of life that necessitated sacrifice. In other mice, the skin abnormality was mild and the mice developed neurological signs (seizure, limb paralysis) that were severe enough to require euthanasia by 4 to 8 weeks. A total of 9 *hGFAP-Cre/Kras^{G12D}/p53$^{fl/fl}$* mice were generated and allowed to age beyond the first post-natal week; at the time of death all 9 had at least focal areas of glioma—a penetrance of 100%. Survival ranged from 30 to 39 days for the animals that were killed due to neurological signs (n = 4).

Examination of the brains of *hGFAP-Cre/Kras^{G12D}/p53$^{fl/fl}$* mice showed bilateral, multifocal, HGGs. Multiple tissue patterns were observed. The patterns were largely pure in a given focus, with 2 or more configurations often abutting one another (Figs. 1B, 2A). One pattern (type A) was virtually identical to that seen with activation of *Kras^{G12D}* alone (18). These foci were characterized by highly infiltrative cells with hyperchromatic, small, oval to angular nuclei with even chromatin and scant cytoplasm (Fig. 1A). Satellitosis of normal, overrun neurons was prominent in this pattern (Fig. 1A). The neoplastic foci, like those in the model with *Kras^{G12D}* alone, involved periventricular areas, particularly the bilateral amygdalohippocampal region (18). Although the histoarchitecture was highly reminiscent of that seen with oncogenic Ras alone, concomitant homozygous deletion of p53 resulted in increased tumor grade, with more cellular foci and increased mitotic activity.

In addition to the type A pattern, other HGG phenotypes were observed simultaneously in the same mouse brain. One distinctive pattern showed cells with abundant, eosinophilic cytoplasm and large vesicular nuclei with prominent nucleoli (Fig. 1C). Another prominent pattern consisted of spindled cells with large, elongated, nuclei and bipolar processes (Fig. 1D). A fourth pattern was characterized by large, often multinucleated"giant" cells (Fig. 1E, F). Still another pattern showed pleomorphic cells of intermediate size with amphophilic cytoplasm (Fig. 1G). Mitoses were readily identified in each pattern. Neither vascular proliferation nor necrosis was present in any configuration.

In addition to distinctive histology on routine hematoxylin and eosin stain, the various patterns differed in protein expression by immunohistochemistry. The most striking difference was in the expression of NSPC/glioma stem cell markers. Cells comprising the type A pattern showed strong nuclear immunoreactivity for Olig2, Sox2 and Bmi-1 (Fig. 2B–D); none of the other patterns showed significant nuclear expression of these NSPC/ glioma stem cell markers (Fig. 2E–G). Nestin expression was particularly prominent in the type A pattern, although all patterns showed some degree of nestin immunoreactivity (data not shown). The type A pattern also showed increased GFAP expression, compared to the other patterns (data not shown).

Foci of Type A Tumor Develop Around the Ventricles and Subventricular Zone as Early as 17 Postnatal Days in *hGFAP-Cre/Kras^{G12D}/p53$^{fl/fl}$* Mice

To assess the location and characteristics of the earliest tumors in *hGFAP-Cre/Kras^{G12D}/p53$^{fl/fl}$* mice, pups were killed at 7, 17, and 21 days. The brains were analyzed with routine and immunohistochemical stains. No abnormalities were detected in 7-day-old transgenic pups, compared to littermate controls. Specifically, no tumor foci were identified (n = 3). Early tumor formation was first seen in 17-day-old mice, with the type A pattern predominating. Type A tumor foci were mitotically active and present near the SVZ (Fig. 3A, a, b; 3B, a, b), in the corpus callosum, and in the anterior commissure. The majority of the cells were strongly immunoreactive for nestin (Fig. 3A, c, d), Olig2 (Fig. 3A, e, f; 3B, b) and Sox2 (data not shown). Ki67 immunohistochemistry labeled the nuclei of these atypical cells (Fig. 3A, g, h). More rarely, foci of other tissue patterns were observed, often in the leptomeninges or cortex (Fig. 3C, a, b). These foci mostly resembled the spindle cell pattern seen in the adult brain. The cells were negative for Olig2 (Fig. 3C, c) and Sox2 (data not shown) expression by immunohistochemistry, although many cells expressed nestin (Fig. 3C, d). Examination of both pups and adult brains by hematoxylin and eosin stain, with multiple brain sections per animal, showed that the type A pattern was contiguous with the ventricle or SVZ in 9/9 (100%) cases. By contrast, non-type A patterns were seen in continuity with the ventricle or SZV in only 3/9 (33.3%) of cases ($p < 0.01$, Fisher exact test, data not shown.

Astrocytes and NSPCs with Oncogenic Ras and Deletion of *p53* Can be Harvested from Neonatal *hGFAP-Cre/Kras^{G12D}/p53$^{fl/fl}$* Mice and Maintained in Culture

To assess differences in tumors derived from NSPC versus more mature astrocytes, cells were harvested from neonatal *hGFAP-Cre/Kras^{G12D}/p53$^{fl/fl}$* pups. For NSPCs, the SVZ was dissected and the cells were cultured with growth factors in the absence of serum, conditions favoring the growth of NSPCs as neurospheres (26). From the same transgenic pup in some cases, astrocytes were harvested from cortex and grown under standard, adherent conditions.

Both neurospheres and adherent astrocytes grew well under these conditions (Fig. 4A, a–d). Recombination PCR performed on DNA isolated from both neurospheres and adherent astrocytes showed recombination of *Kras^{G12D}* (Fig. 4C). Both control and mutant cells harvested from the SVZ and grown as neurospheres showed strong expression of Olig2, nestin and Sox2. (Fig. 4A, B). Control astrocytes, on the other hand, showed virtually no expression of Olig2 or Sox2 (Fig. 4A, B). Interestingly, transgenic astrocytes harvested from neocortex and grown as adherent monolayers showed increased expression of neural/glioma stem cell markers, including Sox2, nestin, Bmi-1 and Olig2, although at generally reduced levels compared to the neurospheres (Fig. 4A, B).

Mutant NSPCs were further characterized by quantitative RT-PCR for genes associated with differentiation and stemness. mRNA was collected from mutant NSPC after 5 days of exposure to the same serum-containing medium in which astrocytes were grown. Compared to NSPCs in serum-free conditions, NSPCs in serum-containing medium showed evidence of differentiation with upregulation of GFAP and S100B gene expression (astrocytic differentiation), Tuj1 gene expression (neuronal differentiation), and MBP gene expression (oligodendroglial differentiation) ($p < 0.0006$; Fig. 5). Simultaneously, gene expression for markers associated with stemness, including nestin and Olig2, was down regulated in NSPCs exposed to serum ($p < 0.01$; Fig. 5). The trend for reduced Sox2 expression with exposure to serum did not reach statistical significance ($p = 0.07$; Fig. 5). Expression of the Dll3 gene, a marker associated with the proneural GBM subtype was downregulated in NSPC exposed to serum (Fig. 5).

Compared to Transgenic Astrocytes, Transplantation of Mutant NSPCs Results in less Aggressive Tumors that Retain the Capacity for Tri-lineage Differentiation

Single cell suspensions of 100,000 NPSCs or cells grown as adherent astrocytes were injected into the striata of normal adult host mice. Both NSPC- and astrocyte-implanted mice developed tumors. Injection of mutant astrocytes, however, was more likely to result in engraftment (Fig. 6A, 11/14 [78.6%]) astrocyte-injected mice vs. 3/10 (30.0%) NSPC-injected mice, $p = 0.035$, Fisher exact test). In addition the astrocyte tumors were more aggressive and the majority of mice were killed by 50 days post-implantation. In contrast, onset of clinical signs was significantly delayed by approximately 2-fold in NSPC-injected mice (Fig. 6B). Consistent with the more aggressive behavior of the neoplasms derived from astrocytes, these tumors more often showed gross hemorrhage and necrosis (Fig. 6C, e–h) compared to the NSPC tumors (Fig. 6C, a–d).

NSPC-derived neoplasms differed from astrocyte-derived tumors histopathologically and in the expression of stem cell and maturation markers (Fig. 7). Both tumor types were highly infiltrative; NSPC-derived tumors tended to diffusely expand the hemisphere into which they were injected (Fig. 7A, a). These tumors were characterized by sheets of cells with round, vesicular nuclei, prominent nucleoli, and moderate amounts of amphophilic cytoplasm (Fig. 7A, b). Giant or spindled cells were rare.

The astrocyte-derived tumors were highly infiltrative into brain parenchyma, often crossing the corpus callosum to involve the contralateral hemisphere (Fig. 7A, i). In one case, the tumor cells had migrated anteriorly to involve the olfactory bulb (data not shown). Tumor cells were present in the ventricular system and the leptomeninges (Fig. 7A, i). Both a spindle cell pattern and a giant cell pattern were seen. The spindled nuclei were often arranged in parallel, forming fascicles of tumor cells. Admixed or in separate foci, large multinucleated cells with abundant eosinophilic cytoplasm were seen (Fig. 7A, j). The mean number of mitoses per HPF in astrocyte-derived tumors was nearly double that of the NSPC tumors (Fig. 7C; $p = 0.004$, Student t-test).

Immunohistochemical and Western blot analyses showed additional differences between astrocyte- and NSPC-derived tumors. In general, compared to the astrocyte-derived neoplasms, the NSPC-derived tumors showed expression of more markers associated with stemness, as well as evidence of multilineage differentiation. Both NSPC- and astrocyte-derived tumors showed GFAP expression, the magnitude of which was greater in the astrocyte neoplasms (Fig. 7A, f, n; B). NSPC tumors also showed Tuj1 and O4 expression, markers of neuronal and oligodendroglial differentiation, respectively, indicating trilineage differentiation (Fig. 7A, g; 7B). The latter markers were not expressed in the astrocyte tumors. Olig2 expression was considerably greater in the NSPC tumors (Fig. 7A, e, m; 7B), whereas Bmi-1 was expressed strongly in both tumor types (Fig. 7B).

Tumorigenic Astrocytes Show a Mesenchymal Gene Expression Pattern, Whereas NSPCs Show a Proneural Gene Expression Pattern

Phillips et al identified a subset of genes in human HGG specimens, expression of which distinguishes among the mesenchymal and proneural tumor subclasses (16). CD44, CHI3L1/YKL-40, and vascular endothelial growth factor (VEGF) gene expression was associated with the mesenchymal phenotype, whereas high brevican (BCAN), and delta-like ligand 3 (DLL3) expression characterized proneural tumors. We designed probes for these genes and performed quantitative RT-PCR on mRNA from cell lysates. For these studies, both mutant NSPC and astrocytes were exposed to the same serum-containing medium. Compared to the tumorigenic NSPCs, gene expression for the mesenchymal markers was markedly elevated in the mutant astrocytes ($p < 0.0005$; Fig. 8). In contrast, BCAN gene expression was higher

in the mutant NSPCs (p = 0.02; Fig. 8). Although differences in DLL3 gene expression were not statistically significant (data not shown), the Tuj1 mRNA level was higher in the mutant NSPCs, suggesting greater early neuronal differentiation (p = 0.006; Fig. 8).

DISCUSSION

The histopathologic diversity of glioblastoma is a hallmark of these neoplasms. In addition, recent advances have shown that high-grade gliomas may be subdivided, based on gene expression profiling, into at least 3 subgroups (16). Furthermore, the neoplastic cells that comprise high-grade glioma are heterogeneous functionally (with a subset of cells that appears to be exceptionally tumorigenic in xenograft assays) has properties similar to tissue stem cells and may be resistant to standard chemoradiation therapies (12, 27, 28). These findings, in addition to the documented presence of endogenous NSPCs in the normal mammalian brain, suggest the possibility that neoplastic transformation of NSPCs could mediate the diversity observed in these neoplasms, and that the differentiation status of the transformed cell, at least in part, determines the phenotype of the resulting neoplasm.

It is well established that the *hGFAP-Cre* transgene directs recombination to multiple cell types, including NSPCs of the SVZ, via mechanisms that include embryonic recombination in radial glia, expression of GFAP in type B cells of the SVZ, and expression of GFAP in mature astrocytes (8, 23, 29–32). Here we show that *hGFAP-Cre*-mediated activation of $Kras^{G12D}$ and homozygous deletion of *p53* results in multiple, spatially distinct, HGG phenotypes that closely resemble several well-known human glioma variants. One phenotype arises near the SZV and marks strongly with NPSC and glioma stem cell markers. Orthotopic transplantation of transformed NSPCs results in a neoplasm with markedly different histology, aggressiveness and protein expression compared to injected astrocytes with identical genetic manipulations. These data indicate that cell of origin may partly determine the histologic heterogeneity seen in human HGG, and suggest that those derived from transformation of endogenous NSPCs may be distinct biologically from those derived from terminally differentiated cells.

The oncogenic stimuli in our model involve activation of the Ras pathway and homozygous deletion of the tumor suppressor p53. The Ras and p53 pathways are critically important in the pathogenesis of glioma. Although Ras mutations are infrequent in glioma, mutations and/or overexpression of upstream activators, such as EGF receptor and platelet-derived growth factor, occur in 88% percent of human glioma specimens (33). In addition, inactivating mutations in the neurofibromin 1 gene, a Ras inhibitor, are associated with heritable glioma-prone syndromes, (e.g. neurofibromatosis type 1), as well as spontaneous tumors (33, 34). Thus, our model is highly relevant to the biology of human disease.

The fidelity with which the infiltrating glioma phenotypes in the hGFAP/ $Kras^{G12D}$ and hGFAP/$Kras^{G12D}$/$p53^{fl/fl}$ models mimic human glioma underscores their biological relevance and usefulness in the study of glioma. In a previous study using the same Cre driver, we showed that activation of $Kras^{G12D}$ alone resulted in intermediate-grade, infiltrating glioma as well as marked hyperplasia of the SVZ (18). The proximity of tumor foci to the expanded SVZ, as well expression of NSPC/glioma stem cell markers in the neoplastic cells, led us to postulate that the tumor cells derived from the SVZ. In the present study, concomitant *p53* deletion in the *hGFAP-Cre*/$Kras^{G12D}$ mouse produced the same cytoarchitectural pattern (dubbed type A, here) seen with oncogenic Ras alone, albeit with increased cellularity and mitotic activity. Namely, the tumor, in architecture, resembled human oligodendroglioma, with a highly infiltrating pattern and satellitosis of normal neurons. Cytologically, however, the tumor cells were more astrocytic in character, with irregularly shaped, hyperchromatic nuclei, resulting in a “mixed” pattern of oligodendroglial

histoarchitecture and astrocytic morphology, a phenotype that is not uncommon in human glioma. As with the tumors arising from activation of *Kras*^{G12D} alone, the tumor cells stained strongly for markers associated with NSPCs and glioma stem cells, and virtually always involved or were closely adjacent to the SVZ or white matter tracts.

Concomitant deletion of p53 not only increased tumor grade in the type A pattern but produced several other distinctly different patterns of HGG that are not present with hyperactive Ras signaling alone. These patterns were spatially distinct and generally non-overlapping in the same mouse. One prominent pattern was highly reminiscent of human giant cell glioma, characterized by huge cells with multinucleated, bizarre nuclei and abundant cytoplasm. Spindle cell patterns as well as “gemistocytic” patterns were also present. In addition to these stark differences histologically, the tumor patterns were distinguished at the level of protein expression. In particular, cells of the type A pattern showed high levels of Olig2, Bmi-1, Sox2 and nestin. Although all the other patterns showed some degree of nestin expression, there was virtually no expression of Olig2, Bmi-1 or Sox2 in cells that comprised any pattern other than type A.

The diversity of glioma phenotypes in a single transgenic mouse could arise from several potential mechanisms. Cells transformed by activation of *Kras*^{G12D} and deletion of *p53* could acquire additional genetic abnormalities that mediate a particular histologic phenotype as well as the expression of NSPC and glioma stem cell markers. Precocious tumor development, including the presence of two or more patterns at postnatal day 17, provides little time for the acquisition of additional mutations, however. Alternatively, the microenvironment in the various regions of the brain could influence the phenotypic expression of Ras pathway activation and *p53* deletion. Finally, the differentiation status of the cell of origin might modulate the phenotypic effects of transgene recombination.

To begin to address these potential mechanisms for the diversity of tumor phenotypes in hGFAP/*Kras*^{G12D}/*p53*$^{fl/fl}$ mice, we isolated NSPC by harvesting forebrain, periventricular tissue from neonatal (less than 7 days old) transgenic pups. From the same brain in many instances, we harvested forebrain cortical astrocytes. Both early passage (less than 10) NSPCs and astrocytes from GFAP/*Kras*^{G12D}/*p53*$^{fl/fl}$ pups formed tumors when they were injected into the striata of host mice. The ability of both cell types to form tumors clearly indicates that they are transformed. Thus, differences in the behavior of tumors arising from transplanted NSPCs versus astrocytes can be attributed to the differentiation status of the transformed cell.

Major differences were seen between astrocyte- and NSPC-derived tumors. First, latency to clinical signs and hence death were markedly shorter in the astrocyte tumors. Histologically, the neoplasms were distinct, with astrocyte tumors recapitulating the spindled and giant cell patterns seen in the spontaneous in vivo tumors. Finally, the tumors showed differences in protein expression by immunohistochemistry and Western blot. NSPC neoplasms showed expression of GFAP, Tuj1, and O4, indicating retention of the capacity to differentiate along astrocytic, neuronal, and oligodendroglial lines, respectively. Despite expression, prior to implantation, of some markers associated with stemness (nestin, Olig2, Sox2, Bmi-1) in the mutant astrocytes, the resulting tumors failed to show differentiation along neuronal or oligodendroglial lines.

Our finding that NSPCs are capable of forming glioma in response to oncogenic stimuli is in accord with the findings of other groups. Bruggeman and colleagues reported that tumors derived from orthotopic transplantation of Bmi-1-deficient, Ink4a/Arf-null, mutant EFGR-expressing astrocytes showed more aggressive histology compared to mutant NSPCs (35). Uhrbom et al and Dai et al targeted oncogenic stimulation to nestin-expressing precursor

cells versus GFAP-expressing cells using the RCAS/tv—a system has shown that cell of origin determines efficiency of tumorigenesis as well as histopathology (36, 37). More recently, Barrett et al used similar methods (including a constitutively active Kras oncogene) to generate HGGs, from which they subsequently separated low and high ID1-expressing tumor cells for orthotopic transplant (38). High ID1-expressing cells showed features associated with stem cells including self-renewal. In transplant experiments, however, and similar to our findings, cells with high ID1-expression showed lower engraftment rates and longer latency to tumor formation. On the other hand, Bachoo et al, with a constitutively active form of EGF receptor, transformed neurospheres and astrocytes harvested from embryonic *Ink4a/arf*-null mice (17). Similar to our data, the astrocytes showed evidence of "dedifferentiation," including upregulation of NSPC markers. However, there was no difference in the capacity for transformed neurospheres and astrocytes to form tumors upon transplantation, and both cell types gave rise to a common glioma phenotype. The discordant result could be due to the different transgenes used to transform the cells or the different age at which the cells were harvested.

The source of stem-like tumor cells within human HGGs has been the subject of debate (10, 11). In concept, the stem-like behavior of these cells might be explained by transformation of endogenous neural stem cells, resulting in unchecked proliferation with retention of multipotency and the capacity for self-renewal. Alternatively, neoplastic transformation in mature glial cells could result in dedifferentiation and reactivation of developmental programs that underlie stem cell-like behavior. These potential mechanisms are not mutually exclusive, and our data do not distinguish among them. Our results do show that neoplasms can arise from transformed NSPCs and that these tumors have distinct biology compared to tumors derived from transformed astrocytes. Although the NSPC-derived neoplasms retained many of the NSPC markers that were present in the cultured cells prior to transplantation, they also showed evidence of multilineage differentiation. On the other hand, prior to transplantation, the transformed astrocytes showed increased neural stem cell markers (nestin, Olig2, Sox2 and Bmi-1) compared to control astrocytes, indicating that transformation with oncogenic Ras and *p53* deletion can upregulate these proteins associated with stemness in differentiated astrocytes.

Studies in human HGG have established 3 subclasses based on gene expression profiling (16). The "mesenchymal" subclass shows upregulation of genes associated with neural stem cells and mesenchymal tissues. The "proliferative" subclass is characterized by expression of genes associated with transit amplifying neural progenitor cells and cellular proliferation. "Proneural" gliomas show a gene expression profile linked to neural differentiation that is similar to that seen in fetal and adult brain. In addition, the proneural profile is associated with markedly increased survival in human patients.

Although the factors that determine the expression pattern and hence molecular classification of a given HGG are uncertain, similarities in glioma phenotype and stages of adult forebrain neurogenesis suggest the hypothesis that cell of origin may be an important factor (16). Indeed, gene expression studies in our mutant NSPCs and astrocytes show striking parallels to the human proneural-mesenchymal axis, with astrocytes showing high levels of gene expression for mesenchymal markers and NSPCs showing elevated BCAN gene expression and early neuronal differentiation. Thus, our data support the hypothesis that the differentiation status of the transformed cell is one determinant of glioma phenotype. The neuronal differentiation, BCAN expression and increased survival in our NSPC-derived tumors parallel the proneural human phenotype, whereas the spindled morphology, expression of stemness and mesenchymal markers, and aggressive nature of the astrocyte-derived gliomas invite comparison to the mesenchymal/stem cell class. Further human and animal studies are required to determine the relationships among cell of origin

and the predominant gene expression signature in glioma. Such studies may contribute to refinement of glioma classification, and, ultimately, uncover novel therapeutic targets.

Acknowledgments

The authors thank Drs. Michael K. Cooper and Harold L. Moses for helpful comments on the manuscript, Dr. Hideaki Ijichi for assistance with *Kras*^{G12D} recombination PCR, Ms. Jean McClure for assistance with the manuscript and figures, and Ms. Jennifer Harvey and Ms. Tracie Moss for expert histological service.

Funding: NIH/NCI T32-CA009592 (SOG) and NIH/NINDS 1 K08 NS062107 (TWA).

REFERENCES

1. Coppola AR. Circumscribed "giant-cell" glioblastoma. Va Med Mon (1918). 1970; 97:753–757. [PubMed: 4367552]
2. Peraud A, Watanabe K, Schwechheimer K, et al. Genetic profile of the giant cell glioblastoma. Lab Invest. 1999; 79:123–129. [PubMed: 10068201]
3. Krouwer HG, Davis RL, Silver P, et al. Gemistocytic astrocytomas: a reappraisal. J Neurosurg. 1991; 74:399–406. [PubMed: 1993905]
4. Meis JM, Martz KL, Nelson JS. Mixed glioblastoma multiforme and sarcoma. A clinicopathologic study of 26 radiation therapy oncology group cases. Cancer. 1991; 67:2342–2349. [PubMed: 1849447]
5. Morantz RA, Feigin I, Ransohoff J 3rd. Clinical and pathological study of 24 cases of gliosarcoma. J Neurosurg. 1976; 45:398–408. [PubMed: 956876]
6. Perry A, Aldape KD, George DH, et al. Small cell astrocytoma: an aggressive variant that is clinicopathologically and genetically distinct from anaplastic oligodendroglioma. Cancer. 2004; 101:2318–2326. [PubMed: 15470710]
7. Lehman NL. Central nervous system tumors with ependymal features: a broadened spectrum of primarily ependymal differentiation? J Neuropathol Exp Neurol. 2008; 67:177–188. [PubMed: 18344909]
8. Doetsch F, Caille I, Lim DA, et al. Subventricular zone astrocytes are neural stem cells in the adult mammalian brain. Cell. 1999; 97:703–716. [PubMed: 10380923]
9. Quinones-Hinojosa A, Sanai N, Soriano-Navarro M, et al. Cellular composition and cytoarchitecture of the adult human subventricular zone: a niche of neural stem cells. J Comp Neurol. 2006; 494:415–434. [PubMed: 16320258]
10. Sanai N, Alvarez-Buylla A, Berger MS. Neural stem cells and the origin of gliomas. N Engl J Med. 2005; 353:811–822. [PubMed: 16120861]
11. Stiles CD, Rowitch DH. Glioma stem cells: a midterm exam. Neuron. 2008; 58:832–846. [PubMed: 18579075]
12. Singh SK, Clarke ID, Terasaki M, et al. Identification of a cancer stem cell in human brain tumors. Cancer Res. 2003; 63:5821–5828. [PubMed: 14522905]
13. Yuan X, Curtin J, Xiong Y, et al. Isolation of cancer stem cells from adult glioblastoma multiforme. Oncogene. 2004; 23:9392–9400. [PubMed: 15558011]
14. Galli R, Binda E, Orfanelli U, et al. Isolation and characterization of tumorigenic, stem-like neural precursors from human glioblastoma. Cancer Res. 2004; 64:7011–7021. [PubMed: 15466194]
15. Ignatova TN, Kukekov VG, Laywell ED, et al. Human cortical glial tumors contain neural stem-like cells expressing astroglial and neuronal markers in vitro. Glia. 2002; 39:193–206. [PubMed: 12203386]
16. Phillips HS, Kharbanda S, Chen R, et al. Molecular subclasses of high-grade glioma predict prognosis, delineate a pattern of disease progression, and resemble stages in neurogenesis. Cancer Cell. 2006; 9:157–173. [PubMed: 16530701]
17. Bachoo RM, Maher EA, Ligon KL, et al. Epidermal growth factor receptor and Ink4a/Arf: convergent mechanisms governing terminal differentiation and transformation along the neural stem cell to astrocyte axis. Cancer Cell. 2002; 1:269–277. [PubMed: 12086863]

18. Abel TW, Clark C, Bierie B, et al. GFAP-Cre-mediated activation of oncogenic K-ras results in expansion of the subventricular zone and infiltrating glioma. Mol Cancer Res. 2009; 7:645–653. [PubMed: 19435821]
19. Uhrbom L, Dai C, Celestino JC, et al. Ink4a-Arf loss cooperates with KRas activation in astrocytes and neural progenitors to generate glioblastomas of various morphologies depending on activated Akt. Cancer Res. 2002; 62:5551–5558. [PubMed: 12359767]
20. Holland EC, Celestino J, Dai C, et al. Combined activation of Ras and Akt in neural progenitors induces glioblastoma formation in mice. Nat Genet. 2000; 25:55–57. [PubMed: 10802656]
21. Jacques TS, Swales A, Brzozowski MJ, et al. Combinations of genetic mutations in the adult neural stem cell compartment determine brain tumour phenotypes. EMBO J. 2010; 29:222–235. [PubMed: 19927122]
22. Jackson EL, Willis N, Mercer K, et al. Analysis of lung tumor initiation and progression using conditional expression of oncogenic K-ras. Genes Dev. 2001; 15:3243–3248. [PubMed: 11751630]
23. Zhuo L, Theis M, Alvarez-Maya I, et al. hGFAP-cre transgenic mice for manipulation of glial and neuronal function in vivo. Genesis. 2001; 31:85–94. [PubMed: 11668683]
24. Smyth GK. Linear models and empirical bayes methods for assessing differential expression in microarray experiments. Stat Appl Genet Mol Biol. 2004; 3 Article3.
25. Benjamini Y, Hochberg Y. Controlling the False Discovery Rate - a Practical and Powerful Approach to Multiple Testing. Journal of the Royal Statistical Society Series B-Methodological. 1995; 57:289–300.
26. Reynolds BA, Weiss S. Generation of neurons and astrocytes from isolated cells of the adult mammalian central nervous system. Science. 1992; 255:1707–1710. [PubMed: 1553558]
27. Rich JN. Cancer stem cells in radiation resistance. Cancer Res. 2007; 67:8980–8984. [PubMed: 17908997]
28. Bao S, Wu Q, McLendon RE, et al. Glioma stem cells promote radioresistance by preferential activation of the DNA damage response. Nature. 2006; 444:756–760. [PubMed: 17051156]
29. Malatesta P, Hack MA, Hartfuss E, et al. Neuronal or glial progeny: regional differences in radial glia fate. Neuron. 2003; 37:751–764. [PubMed: 12628166]
30. Doetsch F, Garcia-Verdugo JM, Alvarez-Buylla A. Cellular composition and three-dimensional organization of the subventricular germinal zone in the adult mammalian brain. J Neurosci. 1997; 17:5046–5061. [PubMed: 9185542]
31. Imura T, Kornblum HI, Sofroniew MV. The predominant neural stem cell isolated from postnatal and adult forebrain but not early embryonic forebrain expresses GFAP. J Neurosci. 2003; 23:2824–2832. [PubMed: 12684469]
32. Zhu Y, Guignard F, Zhao D, et al. Early inactivation of p53 tumor suppressor gene cooperating with NF1 loss induces malignant astrocytoma. Cancer Cell. 2005; 8:119–130. [PubMed: 16098465]
33. Cancer Genome Atlas Research Network. Comprehensive genomic characterization defines human glioblastoma genes and core pathways. Nature. 2008; 455:1061–1068. [PubMed: 18772890]
34. Zhu Y, Parada LF. The molecular and genetic basis of neurological tumours. Nat Rev Cancer. 2002; 2:616–626. [PubMed: 12154354]
35. Bruggeman SW, Hulsman D, Tanger E, et al. Bmi1 controls tumor development in an Ink4a/Arf-independent manner in a mouse model for glioma. Cancer Cell. 2007; 12:328–341. [PubMed: 17936558]
36. Dai C, Celestino JC, Okada Y, et al. PDGF autocrine stimulation dedifferentiates cultured astrocytes and induces oligodendrogliomas and oligoastrocytomas from neural progenitors and astrocytes in vivo. Genes Dev. 2001; 15:1913–1925. [PubMed: 11485986]
37. Uhrbom L, Kastemar M, Johansson FK, et al. Cell type-specific tumor suppression by Ink4a and Arf in Kras-induced mouse gliomagenesis. Cancer Res. 2005; 65:2065–2069. [PubMed: 15781613]
38. Barrett LE, Granot Z, Coker C, et al. Self-renewal does not predict tumor growth potential in mouse models of high-grade glioma. Cancer Cell. 2012; 21:11–24. [PubMed: 22264785]

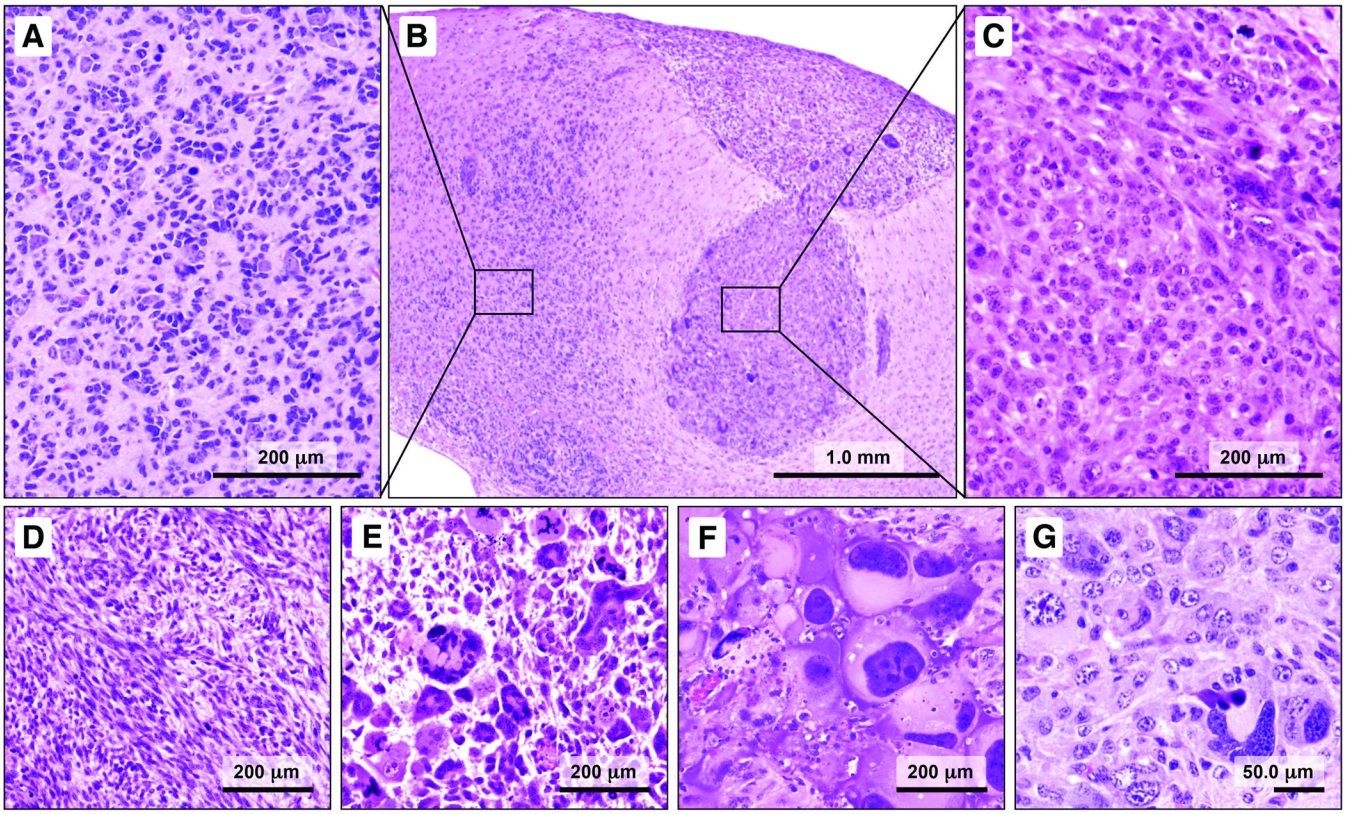

Figure 1.

Multiple high-grade gliomas (HGGs) phenotypes are recapitulated in a single *hGFAP-Cre/Kras*^{G12D}*/p53*$^{fl/fl}$ mouse. (**A–G**) One pattern (type A) consists of cells with small angular nuclei and scant cytoplasm (**A, B**). Satellitosis of overrun, normal appearing neurons and blood vessels is prominent in this pattern. An adjacent focus is composed of neoplastic cells that resemble the large cells of human gemistocytic astrocytoma (**B, C**). In other areas, the tumor cells are distinctly spindled and arranged in fascicles (**D**). Variations in a giant cell pattern also were observed, with bizarre, multinucleated cells with abundant eosinophilic cytoplasm (**E, F**). Other areas showed strikingly pleomorphic nuclei, basophilic cytoplasm, and less distinct cell borders (**G**).

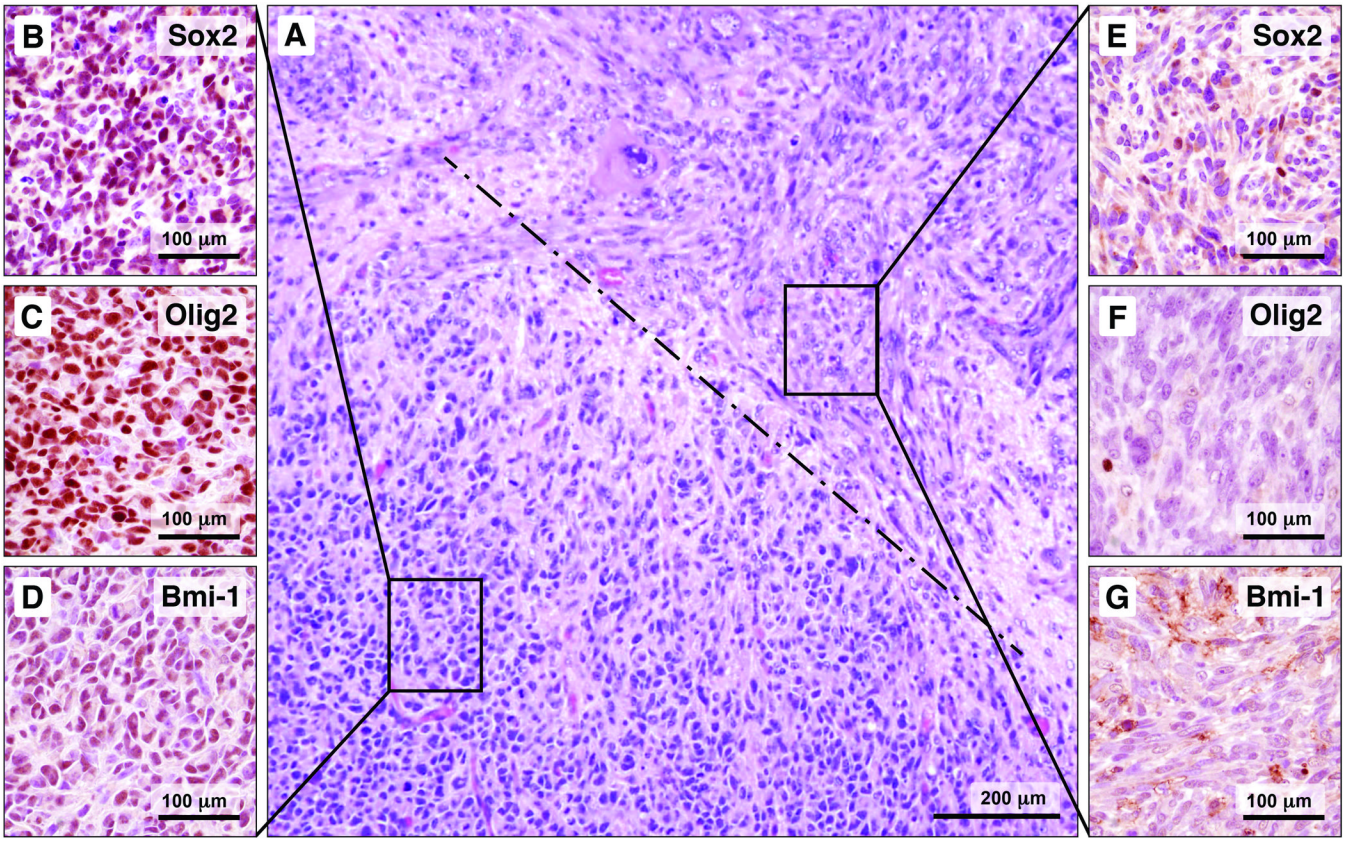

Figure 2.

The high-grade gliomas (HGGs) patterns are geographically distinct; the type A pattern is distinguished from other patterns by expression of markers associated with neural stem/progenitor cells (NSPCs) and glioma stem cells. (**A**) A photomicrograph at intermediate magnification shows a focus of type A pattern juxtaposed to the spindle cell pattern; the dashed line indicates the border between the patterns. (**B–D**) The type A pattern shows nuclear labeling for Sox2, Olig2, and Bmi-1 (brown reaction product). (**E–G**) The adjacent spindle cell pattern largely lacks nuclear immunoreactivity for these markers.

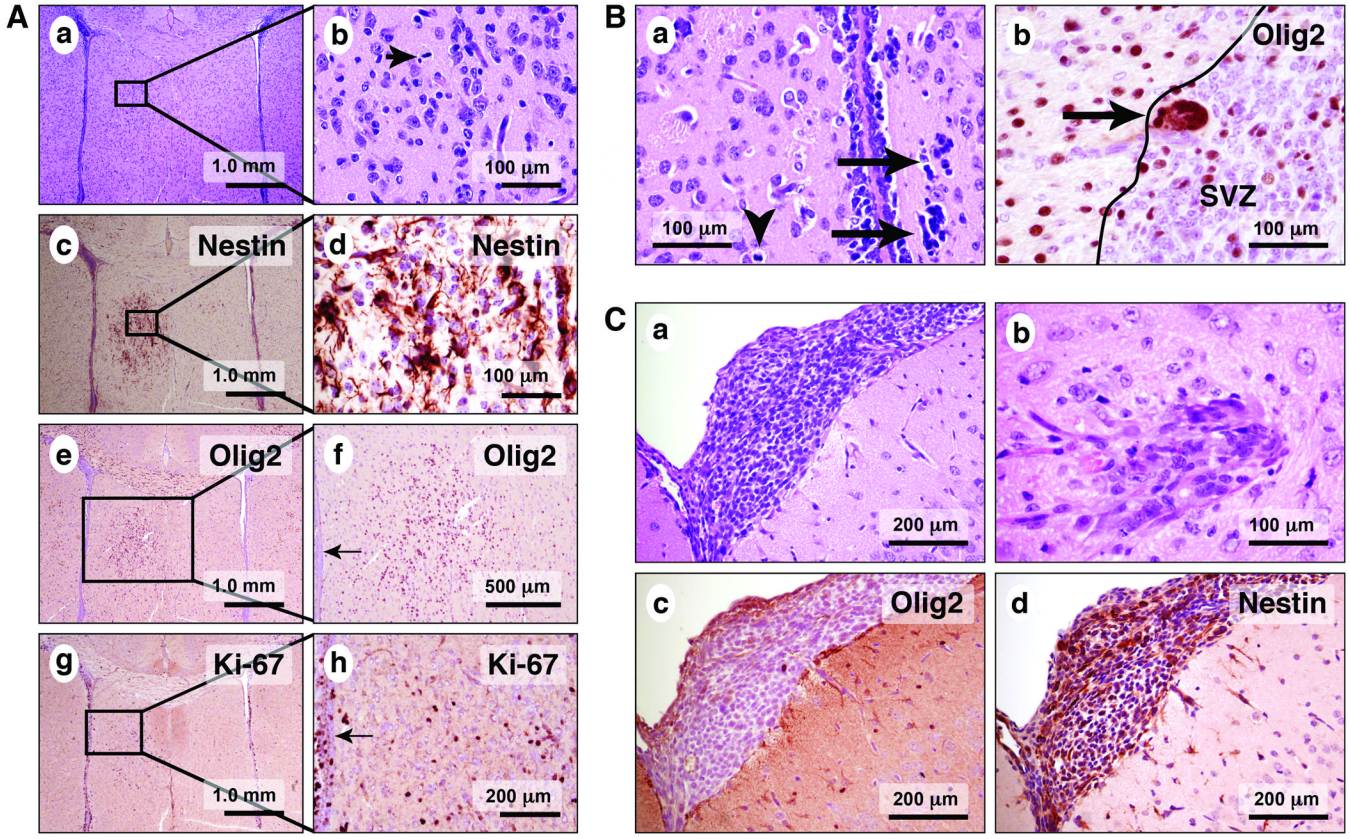

Figure 3.

Microscopic tumor foci are present in *hGFAP-Cre/Kras*^{G12D}*/p53*$^{fl/fl}$ pup brains as early as post-natal day 17. (**A**) The type A pattern is frequently found near the ventricles (**a–h**). (**B**) Cytologically malignant (**a**, arrows) and mitotically active cells (**a**, arrowhead) are present in association with the ependymal lining and the SVZ. The atypical cells are immunoreactive for Olig2 (**b**, arrow). Tumor patterns other than type A are found in 17-day-old pups, including those with leptomeningeal (**a**) and cortical involvement (**b**). Unlike the cells of the type A pattern, the leptomeningeal tumor cells in 3B are negative for Olig2 (**c**), although they are positive for nestin (**d**, brown reaction product).

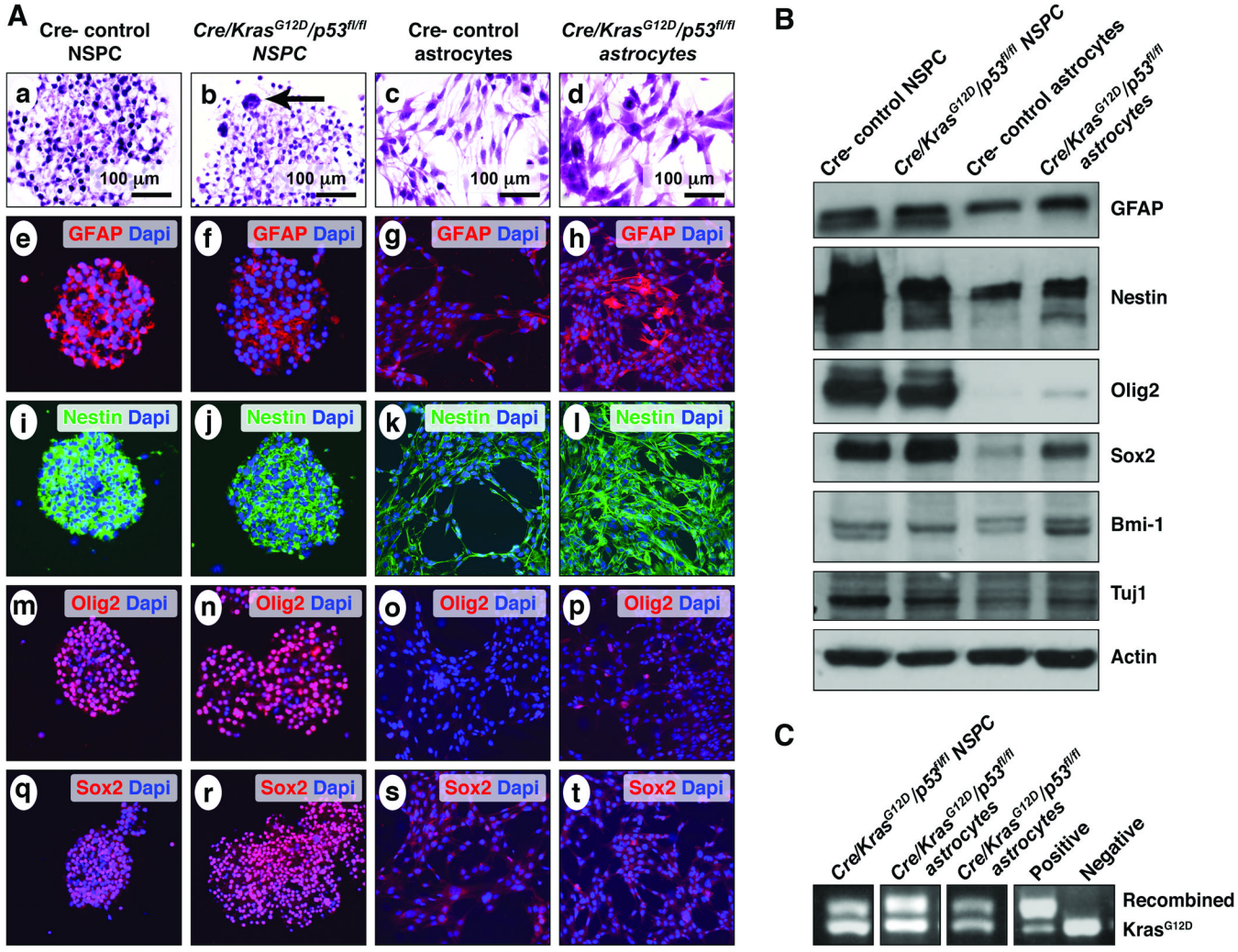

Figure 4.

Characterization of neurospheres and astrocytes harvested from control and mutant neonatal pups. (**A**) Cells harvested from forebrain periventricular areas of both wild type and mutant neonatal mice formed robust neurospheres (**a, b**). Neurospheres from *hGFAP-Cre/Kras^{G12D}/p53$^{fl/fl}$* mice are distinguished from controls on hematoxylin and eosin stain by the presence of scattered, frankly atypical, occasionally multinucleated cells (**b**, arrow). Cortical astrocytes from wild type and mutant pups showed fibrillary processes and often bipolar morphology under adherent conditions (**c, d**). Both control (**e, i, m, q**) and mutant neurospheres (**f, j, n, r**) strongly express neural stem/progenitor cells (NSPC) markers, including glial fibrillary acidic protein (GFAP), nestin, Olig2, and Sox2. In comparison, wild-type astrocytes showed moderate GFAP expression, weak nestin expression and virtually no Olig2 or Sox2 expression (**g, k, o, s**). Astrocytes from *hGFAP-Cre/Kras^{G12D}/p53$^{fl/fl}$* pups, compared to control astrocytes, show similar GFAP expression, increased nestin expression, and scattered Olig2- and Sox2-immunoreactive nuclei (**h, l, p, t**). (**B**) Western blot analysis confirmed the results of the immunofluorescent studies for GFAP, nestin, Olig2 and Sox2. Bmi-1 expression was strongest in the mutant astrocytes (4th lane); Tuj1 expression was strongest in control neurospheres (1st lane). (**C**) PCR shows the presence of the recombined *Kras^{G12D}* allele in a neurosphere line and in 2 adherent astrocyte lines.

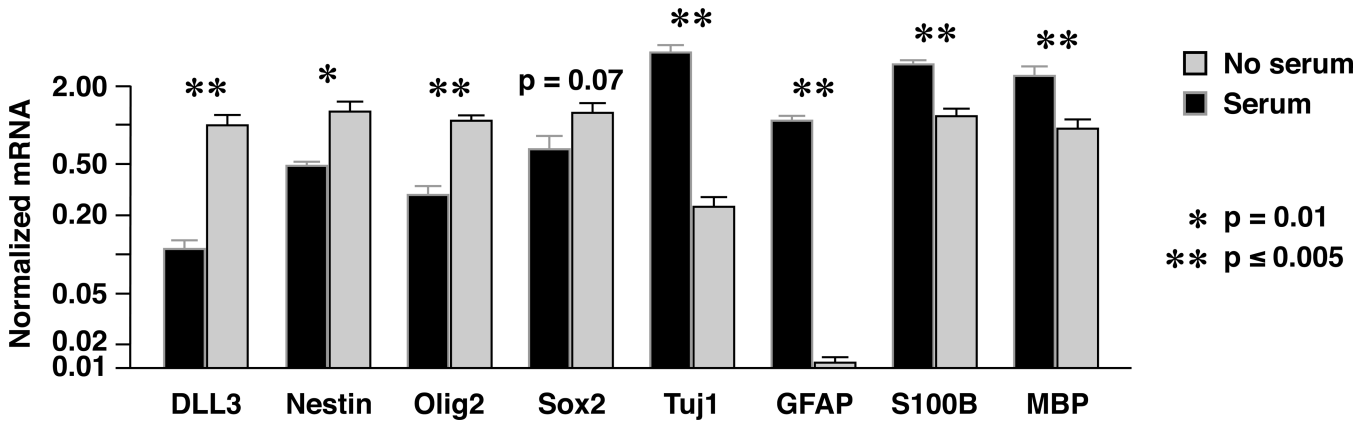

Figure 5.

Mutant neural stem/progenitor cells (NSPCs) exposed to serum-containing medium show downregulation of gene expression for stemness markers and upregulation of genes encoding differentiation markers. *adjusted p value = 0.01. **adjusted p value < 0.005.

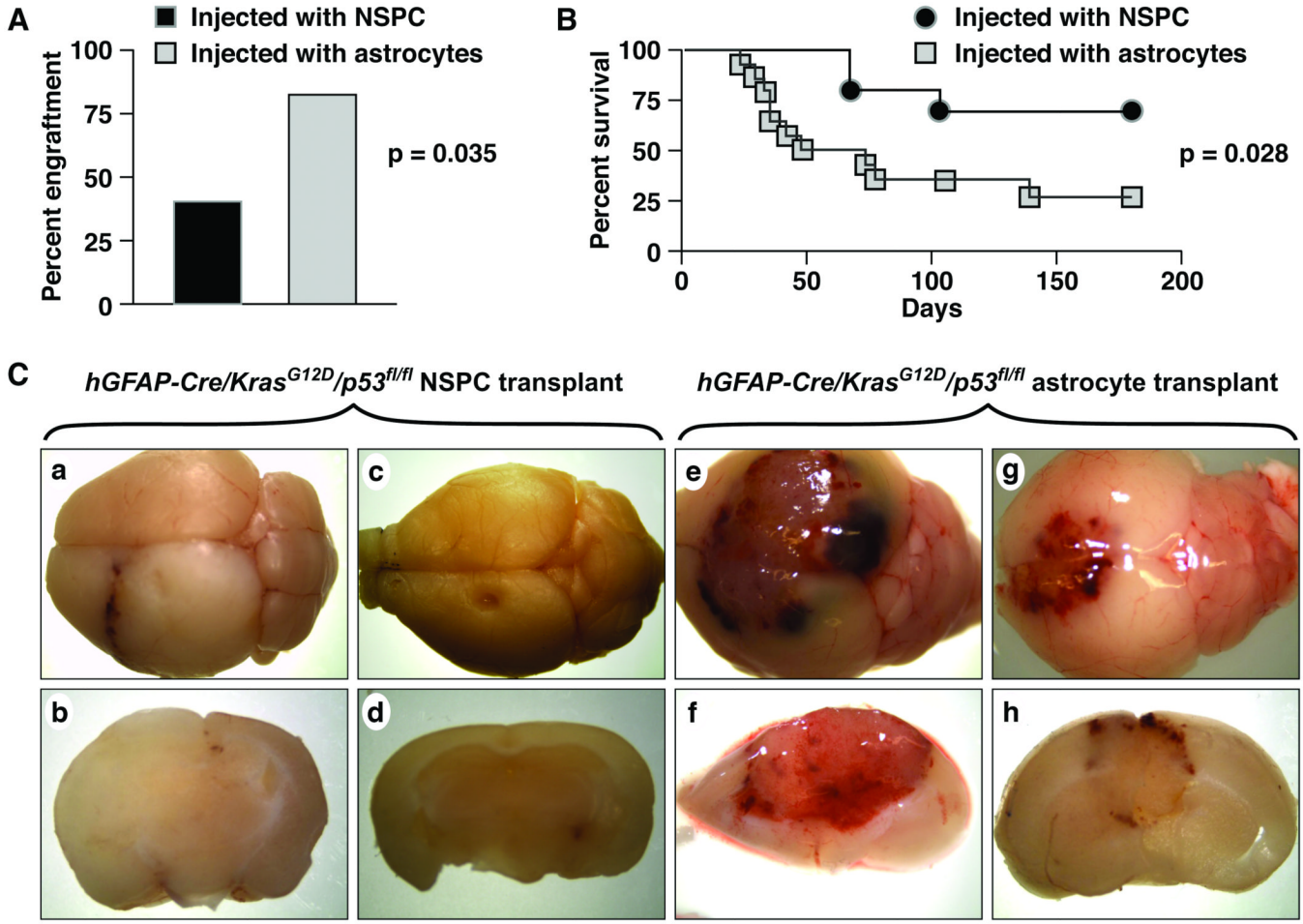

Figure 6.

hGFAP-Cre/Kras^{G12D}/p53$^{fl/fl}$ astrocytes show enhanced engraftment and more aggressive biology, compared to *hGFAP-Cre/Kras^{G12D}/p53$^{fl/fl}$* NSPC, in an orthotopic transplant assay. (**A**) 11/14 (78.6%) mice implanted with astrocytes developed clinical signs with engrafted tumors, compared to 3/10 (30.0%) mice implanted with neural stem/progenitor cells (NSPC) (p = 0.035). (**B**) Kaplan-Meier survival curves show that the onset of signs (and hence survival) was delayed in mice that received transformed NSPC (p = 0.028). (**C**) The NSPC tumors (**a–d**) show less hemorrhage than the astrocyte-induced tumors (**e–h**).

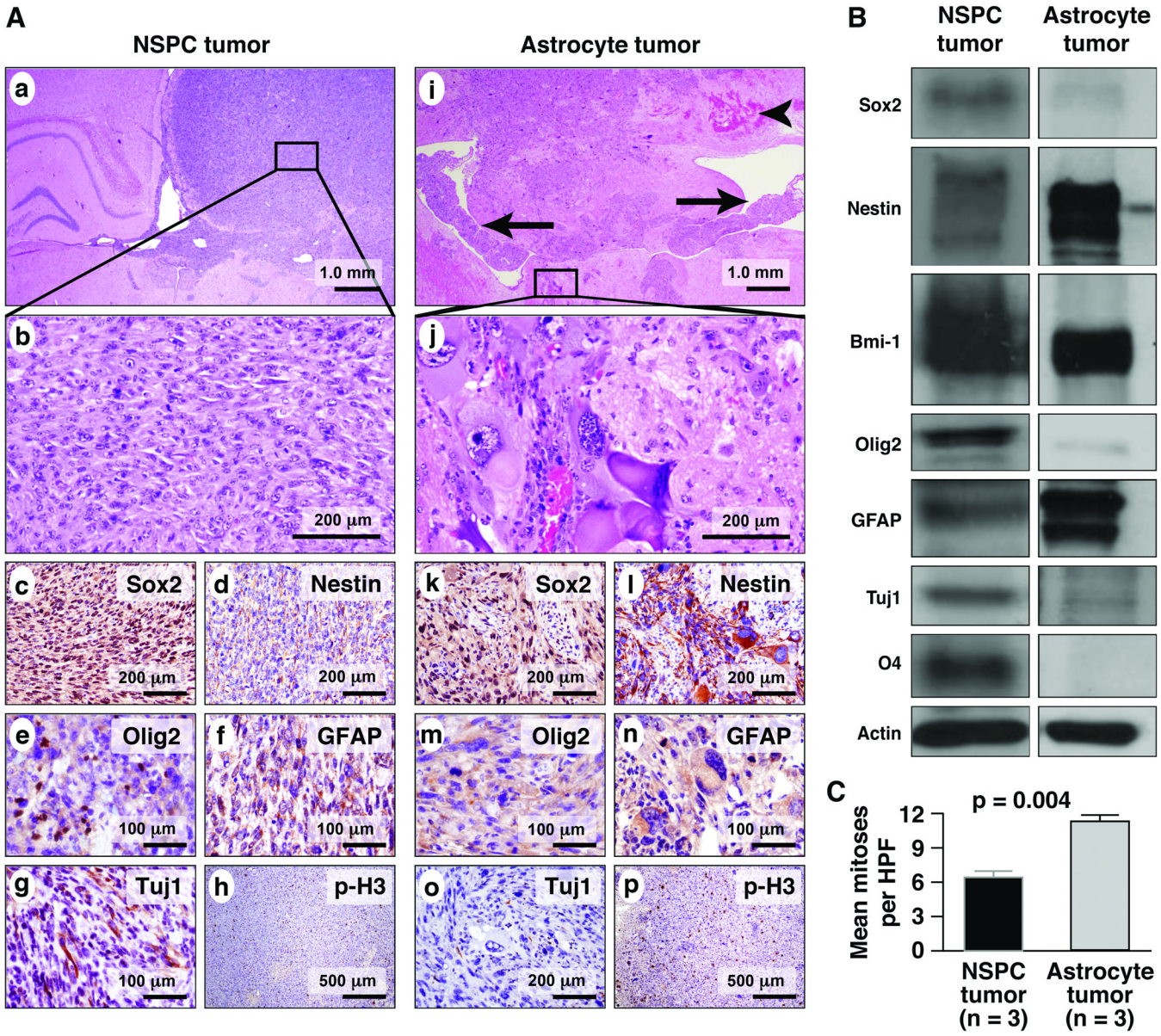

Figure 7.

Tumors that develop after orthotopic transplantation differ histopathologically and show differential protein expression depending on the cell of origin. (**A**) At low magnification, infiltrative tumors arising from mutant neural stem/progenitor cells (NSPC) injection (**a–h**) tend to expand the hemisphere into which they are injected (**a**). A higher magnification view of the NSPC-derived tumor shows a small-cell, spindled cytomorphology (**b**). Sox2 is expressed robustly in the NSPC tumor (**c**, brown reaction product), whereas nestin staining is relatively weak (**d**). Tumors derived from NSPC injections show focal, nuclear Olig2 expression (**e**), moderate glial fibrillary acidic protein (GFAP) expression (**f**) and cytoplasmic Tuj1 expression (**g**). Scattered mitoses are seen with immunohistochemistry for p-H3 (**h**). Tumors derived from implanted astrocytes (**i–p**) are highly infiltrative also, often crossing the corpus callosum to the contralateral hemisphere and involving the ventricles (**i**, arrowhead marks hemorrhage, arrows indicate tumor in the lateral ventricles). Astrocyte tumors are characterized by a prominent giant cell phenotype (**j**). Sox2 expression is weaker

than that seen in NSPC tumors (**k**), while the inverse pattern is seen with nestin (**l**). Olig2 is largely absent in the astrocyte neoplasm (**m**), and there is strong GFAP expression (**n**). Differentiation along neuronal lineages is not detected with Tuj1 in astrocyte tumors (**o**), which have a high mitotic rate (**p**). (**B**) Western blot confirms the immunofluorescent findings in the tumors and shows, in addition, strong Bmi-1 expression in both tumors and O4 expression exclusively in the NSPC tumor. (**C**) Mean mitoses per high-power field (HPF) is significantly greater in the astrocyte-derived neoplasms ($p = 0.004$, Student t-test).

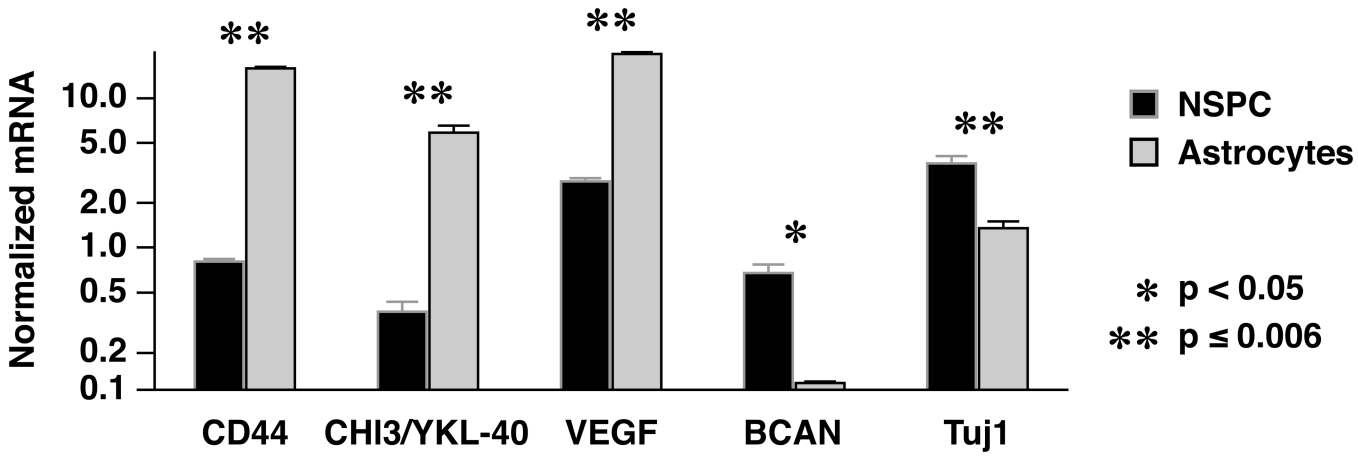

Figure 8.

In serum-containing medium, mutant astrocytes show a pattern of gene expression that parallels that reported for the mesenchymal subclass of human glioblastoma (GBM), including high CD44, CHI3/YKL-40, and vascular endothelial growth factor (VEGF) gene expression. Tumorigenic neural stem/progenitor cells (NSPCs), on the other hand, show a pattern reminiscent of the human proneural subclass, with high brevican (BCAN) and Tuj1 gene expression, compared to the tumors derived from mutant astrocytes. *$p < 0.05$; **$p < 0.006$.